Structure−Function Relations in Self-Assembled C18- and C20-Sphingosines Monolayers at Gas/Water Interfaces

David Vaknin*

Contribution from the Ames Laboratory and Department of Physics and Astronomy, Iowa State University, Ames, Iowa 50011

Received August 27, 2002 ; E-mail: vaknin@ameslab.gov

Abstract: Synchrotron X-ray studies and surface pressure versus molecular area ($\pi-A$) isotherms of C18- and C20-sphingosines spread at air/water interfaces reveal unique interfacial properties with considerable differences between the two single hydrocarbon chain amino-alcohols. C20-sphingosine forms a crystalline monolayer with structural characteristics that are dominated by hydrogen bonding in the headgroup (common to its sphingolipid derivatives), whereas its natural counterpart C18-sphingosine forms a disordered liquidlike metastable monolayer and has to be spread in excess with a floating reservoir on the water surface to compensate for the high dissolution rate of molecules into the water subphase. The marginal affinity of C18-sphingosine to reside at the interface, the microcrystallization at very low densities, the corrugated monolayers it forms, and the strong interaction with the water surface are consistent with the roles that sphingolipids play in the life cycle of eukaryotic cells and as the building blocks of specialized membranes.

Introduction

C18-D-erythro sphingosine is a secondary messenger that mediates cell proliferation and differentiation in mammalian cells[1−3] and is also the building block of a plethora of eukaryotic sphingolipids. For example, ceramides are derived by the acylation of the amino group of sphingosine and are abundant in animals' skin. It was suggested recently that ceramides are active as secondary messengers in regulating cell growth and apoptosis.[1] Substitutions of the terminal hydroxyl group with phosphorylcholine, glucose, and other moieties in sphingosine or ceramides yield sphingomyelin, cerebrosides, gangalosides, and a variety of other sphingolipids. Recent studies show that sphingolipids together with cholesterol can form microdomains that act as rafts for transporting proteins in cells.[4] It is therefore likely that sphingolipids possess unique interfacial properties that enable them to carry out their tasks as messengers and as lipid rafts, such as residing at aqueous interfaces (membranes) but with a relatively high dissolution rate into the bulk water solution (cytoplasm) to interact with specific messengers, and strong mutual binding interactions to form microdomain substrates for proteins to bind.

Here, we report synchrotron X-ray investigations of C18- and C20-D-erythro sphingosines (see Figure 1; C18-SP and C20-SP, respectively) that consist of a single hydrocarbon chain and an amino-alcohol headgroup, differing merely in the length of their hydrocarbon chain. The length of the hydrophobic tail (including a trans double bond between C4 and C5) of C18-SP
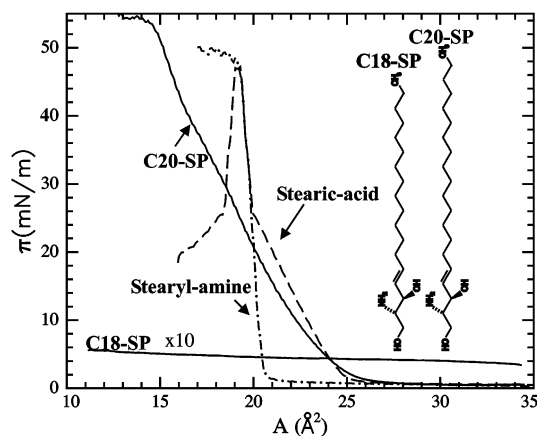
Figure 1. C18-SP and C20-SP molecules used in this study and their $\pi-A$ isotherms on pure water. The C18-SP isotherm shows a very weak increase in pressure upon compression, characteristic of impurities on water surfaces. The surface pressure of C18-SP when spread conventionally does not exceed 0.5 mN/m; however, a metastable monolayer can be formed by depositing the material in excess of a monolayer at the interface. The C20-SP film can maintain high surface pressures, although it does not have sharp transitions to the tilted (short-range order) and nontilted phase commonly observed in fatty acids and alcohols.[5] The dashed line and the dashed dotted line show the isotherms of stearic acid and stearylamine (octadecylamine), respectively. Both of these latter monolayers collapse at $\simeq$45 mN/m at a molecular area of $\simeq$19 Å², which reflects their hydrocarbon chain cross section.

is comparable to that of stearic acid or stearylamine, which self-organize as ordered monolayers at air/water interfaces.[5]

The specific arrangement of molecules in a stable monolayer at the air/water interface depends on a variety of competing interactions, such as van der Waals forces (mainly among

(1) Hannun, Y. A. *J. Biol. Chem.* **1994**, *269*, 3125−3128.
(2) Hauser, J. M.; Buehrer, B. M.; Bell, R. M. *J. Biol. Chem.* **1994**, *269*, 6803−6809.
(3) Spiegel, S.; Merrill, A. H. *FASEB J.* **1996**, *10*, 1388−1397.
(4) Simons, K.; Ikonen, E. Functional rafts in cell membranes. *Nature* **1997**, *387*, 569−572.
(5) Gaines, G. L., Jr. *Insoluble Monolayers at Liquid−Gas Interfaces*; Wiley: New York, 1966.

hydrocarbon tails), ionic and dipolar interactions, hydrogen bonding (headgroup region), and interactions with water molecules. The unique structure of the sphingosine molecule, in particular, its amino-alcohol headgroup, brings about a few of these interactions. It exhibits relatively strong hydrogen bonding among neighboring molecules due to the hydroxyl groups (proton acceptors) and the amine group (proton donor). Recent grazing incidence X-ray diffraction (GIXD) studies of C18-ceramide monolayers revealed that condensation into two-dimensional (2D) crystals occurs at low densities in a region of the $\pi-A$ isotherm ($\pi \approx 0$) that is regularly attributed to the 2D gas phase of monolayers.[6] X-ray reflectivity (XR) results indicated that the ceramide monolayer is severely corrugated at the air/water interface due to the staggering of bound neighboring molecules. It was concluded that these structural differences between ceramide and related lipids result from strong hydrogen bonds present in the headgroup region.[7,8] Subsequent XR and GIXD studies of C18-sphingomyelin monolayers at air/water interfaces led to similar conclusions.[9]

Experimental Details

C18-SP ($C_{18}H_{37}O_2N$; MW = 299.5) and C20-SP ($C_{20}H_{41}O_2N$; MW = 327.6; see Figure 1) were obtained from Matreya, Inc. (Pleasant Gap, PA) (materials have catalog numbers 1802 and 1840 in the Matreya, Inc. catalog #7, 1999−2000). Samples were weighed directly into volumetric flasks and were subsequently filled with chloroform/methanol 2:1 (HPLC grade, Fisher Scientific, Fair Lawn, NJ) and sonicated to form uniform solutions. Langmuir monolayers were prepared on pure water (Milli-Q apparatus Millipore Corp., or Bedford, MA; resistivity, 18.2 MΩ cm) in a temperature-controlled Teflon trough maintained at 19 ± 1 °C enclosed in a gastight aluminum container. The surface pressure was measured with a microbalance using a filter-paper Wilhelmy plate. To reduce incoherent scattering from air and to slow film deterioration by oxidation due to production of radicals by the intense synchrotron beam, the monolayer was kept under a helium environment throughout the X-ray studies. The Langmuir trough is mounted on a motorized stage that can translate the surface laterally with respect to the incident beam for probing different regions of the surface. X-ray measurements were collected at different areas of the surface to monitor possible radiation damage and to determine sample-exposure times to optimize counting rates, using this lateral translational stage.

A newly commissioned liquid surface diffractometer at the Advanced Photon Source (APS), beam-line 6ID-B (described elsewhere[10]), was employed to investigate the structure of monolayers at air/water interfaces. The highly monochromatic beam (16.2 keV; $\lambda = 0.765334$ Å), selected by a downstream Si double crystal monochromator, is deflected onto the liquid surface to a desired angle of incidence with respect to the liquid surface by a second monochromator (Ge(220) crystal) located on the diffractometer.

X-ray reflectivity (XR) and grazing incident X-ray diffraction (GIXD) techniques are commonly used to determine the structure of monomolecular films on molecular length scales. Specular XR experiments yield the electron density profile across the interface and can be related to molecular arrangements in the film. The electron density profile across the interface is extracted by refining a slab model that best fits the measured reflectivity by the nonlinear least-squares method.

The reflectivity from the slab model at a momentum transfer, Q_z, is calculated by

$$R(Q_z) = R_0(Q_z)e^{-(Q_z\sigma)^2} \tag{1}$$

where $R_0(Q_z)$ is the reflectivity from steplike functions calculated by the recursive dynamical method,[11] and σ is an effective surface roughness, accounting for the smearing of all interfaces due to thermal capillary waves and surface inhomogeneities.[10,12] The variable parameters used to construct the electron density across the interface $\rho(z)$ include the thickness values of the various slabs d_i, their corresponding electron densities ρ_i, and one surface roughness parameter.[13]

GIXD experiments are conducted to determine the lateral organization in the film. In these experiments, the angle of the incident beam with respect to water surface, α, is fixed below the critical angle for total reflection, while the diffracted beam is detected at a finite azimuthal in-plane angle, 2Θ, and out-of-plane angle, β. In general, the diffraction pattern from lipid monolayers consists of a few Bragg reflections due to 2D ordering of the hydrocarbon tails.[14] To obtain the average ordered chain length and tilt with respect to the surface normal, out-of-plane scans at the Bragg peak positions (rod-scans) are measured and analyzed using standard procedures.[10,15] The intensity along the rod of the 2D Bragg reflection is analyzed in the framework of the distorted wave Born approximation (DWBA) using[10,16]

$$I(Q_{xy},Q_z) \approx |t(k_{z,i})|^2|F(Q_z)|^2|t(k_{z,f})|^2 \tag{2}$$

where $t(k_{z,i})$ and $t(k_{z,f})$ ($k_{z,i} = k_0 \sin \alpha$; $k_{z,f} = k_0 \sin \beta$) are the Fresnel transmission functions, which give rise to an enhancement around the critical angle [$\alpha_c = \beta_c = \lambda(\rho_s r_0/\pi)^{1/2}$; $r_0 = 2.82 \times 10^{-13}$ cm].

Results and Discussion

Isotherm Comparisons. Surface pressure versus molecular area isotherms for C18-SP and C20-SP are shown and contrasted with those of stearic acid and stearylamine in Figure 1. Although stearic acid and stearylamine exhibit different features in their isotherms, both monolayers collapse at a minimum area that reflects densely packed chains that are nearly normal to the aqueous surface with an average cross section of ~19 Å^2 per chain. The isotherm of C20-SP differs significantly from those of stearic acid and stearylamine, as it consistently collapses at higher surface pressures[17] and at a minimum area significantly smaller than that of a typical hydrocarbon chain cross section. This is suggestive of a finite loss of molecules possibly due to dissolution and/or multilayer formation. By contrast, according to its $\pi-A$ isotherm, C18-SP does not maintain surface pressure that exceeds ~0.5 mN/m and tends to collapse at very low surface pressures. However, as demonstrated below, X-ray scattering studies of spread C18-SP at vanishingly small surface pressures ($\pi \approx 0$) indicated the existence of a monolayer at the air/water interface, albeit a highly disordered one. We argue that this is due to the higher rate of dissolution of the molecules into water. To study films of C18-SP, we adapted an established procedure to produce metastable monolayers at gas/water

(6) Vaknin, D.; Kelley, M. S. *Biophys. J.* **2000**, *79*, 2616−2623.
(7) Löfgren, H.; Pascher, I. *Chem. Phys. Lipids* **1977**, *20*, 273−284.
(8) Bruzik, K. S. *Biochim. Biophys. Acta* **1988**, *939*, 315−326.
(9) Vaknin, D.; Kelley, M. S.; Ocko, B. M. *J. Chem. Phys.* **2001**, *115*, 7697−7704.
(10) Vaknin, D. In *Methods in Materials Research*; Kaufmann, E. N., Abbaschian, P., Barnes, P. A., Bocarsly, A. B., Chien, C.-L., Doyle, B. L., Fultz, B., Leibowitz, L., Mason, T., Sanchez, J., Eds.; Wiley: New York, 2001; p 10d.2.1.
(11) Parratt, L. G. *Phys. Rev.* **1954**, *59*, 359−369.
(12) Als-Nielsen, J.; Kjaer, K. *Proc. NATO ASI Ser. B* **1989**, 211−113.
(13) The number of slabs used to fit the data is the minimum necessary for which an additional slab does not improve the quality of the fit.
(14) Kaganer, V. M.; Möhwald, H.; Dutta, P. *Rev. Mod. Phys.* **1999**, *71*, 779−819.
(15) Kjaer, K. *Physica B* **1994**, *184*, 100−109.
(16) Vineyard, G. *Phys. Rev. B* **1982**, *26*, 4146−4159.
(17) In the present study, C20-SP collapses at 55 mN/m as compared to ~45 mN/m for stearic acid. It should be noted that the pressure of collapse depends on the purity of the surface in addition to the properties of the specific spread monolayers.
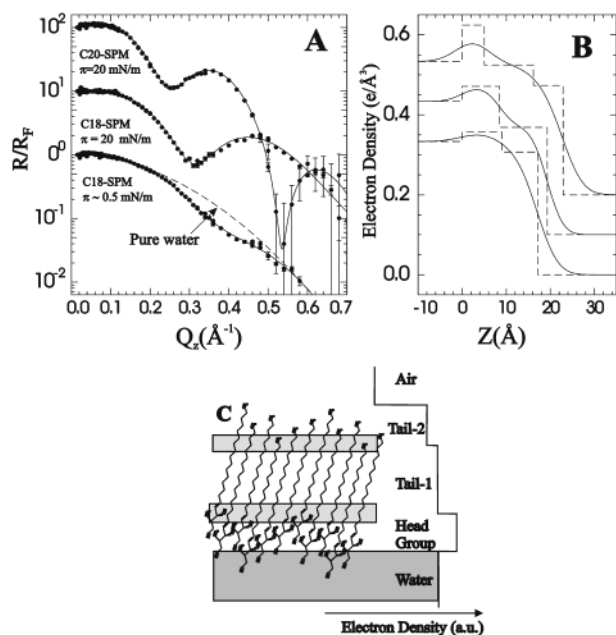
Figure 2. (A) Reflectivities normalized to R_F (R_F is the reflectivity of an ideally flat water surface) from monolayers of C20-SP ($\pi = 20$ mN/m) and of C18-SP ($\pi \geq 0$ mN/m and at 20 mN/m − spread in excess of a single layer). The dashed line is the reflectivity from the water surface, showing the slight deviation of the reflectivity of C18-SP from that of the pure water surface. (B) Electron density profiles (solid lines) used to calculate the reflectivities that best fit the data (solid lines in A). The dashed lines represent the box models, assuming flat interfaces without roughness. (C) A schematic illustration of the C20-SP monolayer and the corresponding electron density profile depicting the corrugation due to disordered amine-hydroxyl hydrogen bonding. The resulting corrugation at the headgroup region leads to a distinct low-density hydrocarbon slab forming random chain digitation. It is found that only the central hydrocarbon slab gives rise to the 2D Bragg reflection observed in the GIXD.

interfaces.[18] It is well known that the dissolution rate of short-chain molecules in a monolayer can be significantly slowed by promoting chain−chain interaction at high surface pressures (i.e., forming them at high densities). To achieve high lateral density, C18-SP is spread from a solution in excess of a single layer (the equivalent of approximately 10 monolayers) at the interface (away from the footprint of the X-ray beam), forming an intact film with a finite surface pressure.

The spreading at a limited region of the trough provides a reservoir of molecules at the interface that compensates for dissolution. This allows for the stabilization of a monolayer with a surface pressure as high as 40 mN/m over the course of the X-ray measurements. A similar approach to forming metastable monolayers of short- and medium-chain alcohols ($C_nH_{2n+1}OH$; $n = 9-16$) with a relatively high dissolution rate from a reservoir at the interface has recently been thoroughly investigated by surface X-ray scattering techniques.[18,19] It has long been known that alkyl chain molecules (fatty acids, fatty amines, fatty alcohols, and others) generally dissolve into water; it is only by virtue of the slow process that these systems exist in this metastable state.[5]

X-ray Reflectivity. Figure 2A shows normalized reflectivity curves, R/R_F (where R_F is the calculated reflectivity of an ideally

(18) Berge, B.; Konovalov, J.; Lajzerowicz, J.; Renault, A.; Rieu, J. P.; Vallade, M.; Als-Nielsen, J.; Grübel, G.; Legrand, J. F. *Phys. Rev. Lett.* **1994**, *73*, 1652−1653.
(19) Zakri, C.; Renault, A.; Rieu, J. P.; Vallade, M.; Berge, B.; Legrand, J. F.; Vignault, G.; Grübel, G. *Phys. Rev. B* **1997**, *55*, 14163−14172.

Table 1. Best-Fit Parameters to the Measured Reflectivities of C18-SP and C20-SP Monolayers that Generate the Two- and Three-Box Models of the Electron Density Profiles Across the Interface

π (mN/m)	d_1 (Å)	ρ_1 (e/Å³)	d_1 (Å)	ρ_1 (e/Å³)	d_1 (Å)	ρ_1 (e/Å³)	σ (Å)	d_{total} (Å)
			C18-Sphingosine					
0.5	9.0	0.357	8.1	0.27			3.7	17.1
30	8.5	0.371	10.8	0.307			2.9	19.3
			C20-Sphingosine					
1	9.5	0.384	10.7	0.328	5.3	0.19	2.6	25.5
10	9.2	0.391	10.8	0.329	5.4	0.22	2.8	25.4
20	9.0	0.381	10.8	0.314	5.7	0.21	3.0	25.5
32	9.0	0.385	10.0	0.315	6.8	0.23	3.5	25.8

flat water interface), for both C18-SP and C20-SP monolayers (A). The solid lines are the best-fit calculated reflectivities based on the ED profile models shown in Figure 2B. For C18-SP, two sets of measurements were performed, one for films that were spread with the intention to form a single layer by compression to a nominal molecular area of approximately 20 Å² ($\pi \approx 0$) and the second using the metastable procedure with excess material at the interface, as described above. Despite the fact that no significant surface pressure build-up is observed upon common compression (i.e., with no excess material at the interface), X-ray reflectivities of C18-SP films show time-dependent deviations from the expected reflectivity of a pure water surface, providing evidence for the presence of varying amounts of C18-SP traces at the aqueous surface. Figure 2A shows a measured reflectivity from one such film of C18-SP, where the dashed line is the best fit to the data assuming a single interface (i.e., water surface only) with an average surface roughness, $\sigma = 2.8$ Å. Analysis of the measured reflectivity in Figure 2A using the two-box model[8,10] shown in Figure 2B yields a total film thickness $d_{total} \approx 17$ Å, as compared to $d_{st} \approx 22.8$ Å estimated for the stretched molecule. The 9 Å slab, near the water, is significantly thicker than the actual molecular headgroup size (5−6 Å), suggesting a collective broadening due to nonsmooth distribution of the amino-alcohol portions of the molecules in this slab. Assuming uniformly distributed molecules at the surface, the film thickness is found to be consistent with an average tilt angle of $t \approx 42°$ with respect to the surface normal ($\cos(t) = d_{total}/d_{st}$). Such a tilt of the molecules has to be at random orientations as in a liquidlike phase, as evidenced by the GIXD below.

Integrating over the electron density profile yields the in-plane electron density of the film, which can be compared to N_e/A, where $N_e = 168$ electrons per C18-SP formula, and A is the average molecular area A in the film, such that

$$A \int \rho(z) \, dz \approx N_e \qquad (3)$$

Using the results in Table 1 and eq 3 yields an estimated molecular area $A = 31.1$ Å² as compared to the area extracted from the GIXD under the same conditions $A_{GIXD}/\cos t \approx 32.3$ Å² ($A_{GIXD} = 23.994$ Å²; it should be noted that, in this estimate, bound water molecules in the film are not accounted for in N_e).

Spreading C18-SP in excess of a single layer to form a metastable monolayer at surface pressures in the 20−40 mN/m range gives rise to reflectivity (Figure 2A) with a prominent minimum at $Q_z = 0.32$ Å⁻¹, indicating the formation of a more homogeneous film at the interface. The films are highly stable
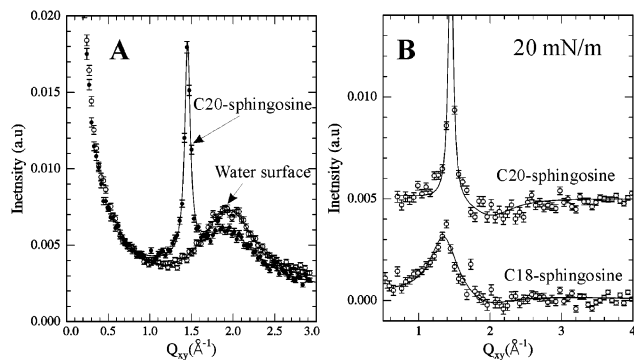
Figure 3. (A) Grazing incidence X-ray diffraction (GIXD) scans for a pure water surface (empty circles), and a C20-SP monolayer at the air/water interface ($\pi = 20$ mN/m). The falloff in intensity at small angles is due to scattering from capillary waves at the interface, whereas the broad peak is due to the structure factor of the water surface, which we find to be slightly different than that of bulk water.[20] (B) The GIXD from monolayers after subtracting the contribution of water is shown for C20-SP and for C18-SP. The diffraction peak at $Q_{xy} = 1.471$ Å^{-1} is due to the ordering of alkyl chains in the C20-SP monolayer as discussed in the text, whereas the broad peak at $Q_{xy} = 1.38$ Å^{-1} is indicative of a 2D liquidlike behavior of C18-SP. Both monolayers show a very weak minimum around $Q_{xy} = 2.0$ Å^{-1}, indicating some reorganization of water at the interface due to headgroup—water interaction.[21]

over the course of the X-ray measurements (several hours), with reproducible reflectivities. The analysis of the reflectivity in terms of a two-box model with a total film thickness of 19.4 Å precludes multilayer formation.

In contrast to C18-SP, the normalized reflectivities of the C20-SP monolayer at finite pressures exhibit two distinct minima characteristic of long-chain fatty acids or alcohols. However, to get the best fit to the reflectivities from C20-SP monolayers, the two-box model is insufficient, and a three-box model is required (Figure 2B). This is, in fact, a common feature of several sphingolipids.[6,7] The model shows that the ED associated with the hydrocarbon chain consists of two distinct densities, as is schematically depicted in Figure 2C. In particular, the top slab at the gas interface has an electron density much lower than that of densely packed hydrocarbon chains (0.31−0.33 e/Å^3), which can result from corrugation on either molecular- or domain-size length scales. The analysis of the rod scans below suggests that the topmost layer is corrugated on a molecular length scale, whereby the chains form a digitated interface as illustrated in Figure 2C. For both C18-SP and C20-SP, the slab associated with the headgroup at the water interface is relatively longer than the amino-alcohol headgroup of sphingosine, reflecting a collective broadening of that region due to staggered hydrogen bonds among neighboring molecules, as suggested earlier.[6,7] It is argued that in conforming to the broadening at the headgroup region, hydrocarbon tails form the corrugation (digitation) at the gas interface. The optimized parameters used to calculate the reflectivities at various pressures are listed in Table 1 for both C18-SP and C20-SP. The parameters in Table 1 indicate that the electron densities of the monolayers are relatively stable and change very little with the compression.

GIXD and Rod Scans from the Monolayer. The lateral organization of C18-SP and C20-SP in monolayers reinforces the conclusions from the reflectivity and the isotherms. The GIXD pattern (for $\beta = 0$) of pure water surfaces is dominated by a broad peak at $Q_{xy} = 1.94$ Å^{-1}, due to the structure factor of the liquid surface, as shown in Figure 3A.[20]
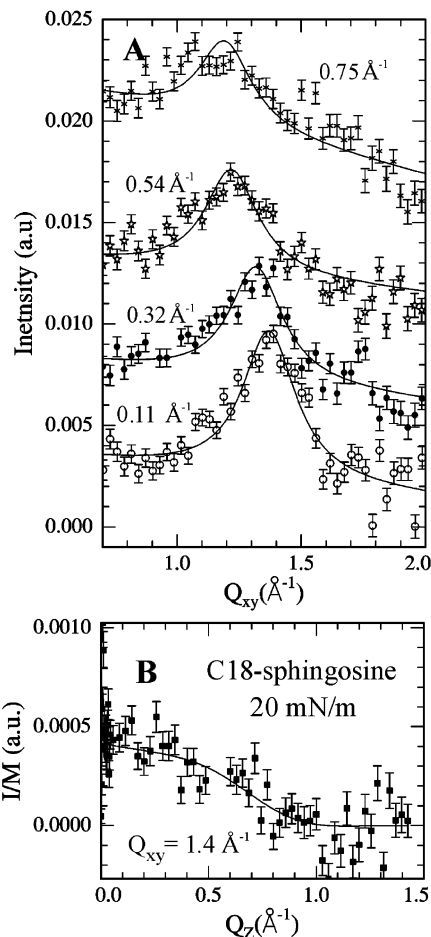

Figure 4. (A) Diffraction patterns from a metastable C18-SP monolayer (20 mN/m) at several $k_{z,f}$ values, as indicated. The gradual shift of peak position as Q_z increases and the small variation in intensity indicate that the monolayer is in a liquid state with no orientational ordering despite the relatively high surface pressure. (B) Rod scan at $Q_{xy} = 1.4$ Å^{-1}. The solid line is a fit to the data assuming short-range order hexagonal symmetry and using a 10.0 Å chain length that is tilted at 23.4° from the surface normal.[21]

Spreading and compressing C18-SP, or C20-SP monolayers, slightly modifies the aqueous surface structure factor, primarily in intensity. For C20-SP at finite pressures, a prominent sharp Bragg peak appears at $Q_{xy} = 1.47$ Å^{-1}. Figure 3B shows the same scan after the subtraction of the GIXD of pure water. Besides the Bragg peak, there is a negative broad minimum due to the modification of the water surface by the monolayer aforementioned. Applying a similar procedure to the C18-SP monolayer yields, in addition to the modification of the water surface structure factor, a broad peak centered at $Q_{xy} = 1.38$ Å^{-1}.

The observation of a broad GIXD peak at and off the horizon for C18-SP together with the rod scans, as shown in Figure 4,

(20) For bulk water, the first peak in the structure factor is observed at $Q_{xy} \approx 2.0$ Å^{-1} as compared to the 1.96 Å^{-1} for water surface. The penetration depth of the incident evanescent X-ray is smaller than 100 Å, thereby probing the topmost water layers with some contribution from bulk liquid. The shift in the position of the first peak indicates a slightly larger O−O d spacing at the interface.

(21) The typical intensity of the incident beam illuminating the sample is 10^{11} photons/s (through a sample slit approximately 1 × 0.1 mm^2). Counting time for GIXD measurements was 1−4 s per point, whereas for the rod scans, it varied between 4 and 20 s per point. The data shown in Figures 3−6 were all normalized to a monitor before the sample with an average 68 000 counts/s. For example, at the count rate of the peak of the Bragg reflection of C20-SP (Figure 3A), it is nearly 1200 counts/s.
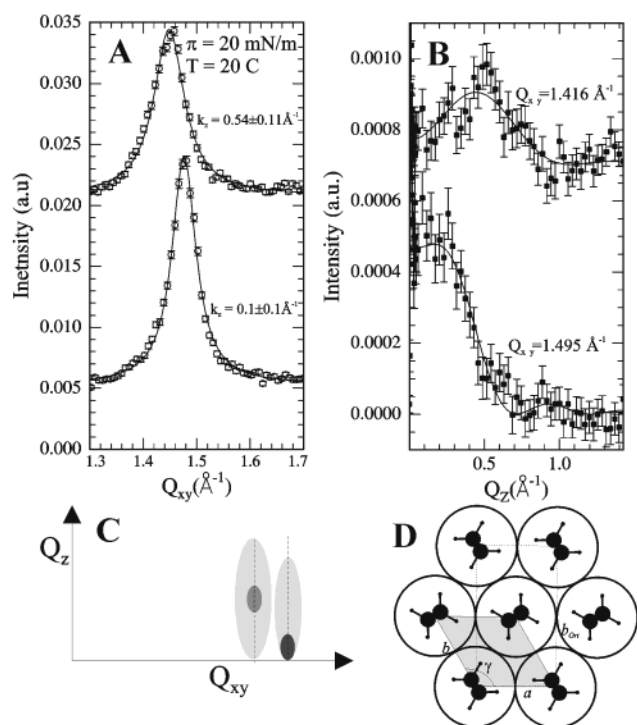
Figure 5. (A) Diffraction patterns for C20-SP showing two distinct peaks at two $k_{z,f}$ values. The two peaks are due to the rhombic symmetry (equivalent to centered rectangular) of the ordered hydrocarbon chains. (B) Rod scans at the two Bragg peaks are shown in (A). Best-fit analysis (solid line) of the intensity along the rod yields a uniform $18 \pm 3°$ tilt angle of chains with respect to the surface normal. (C) Schematic map of reciprocal space showing the position of the two Bragg reflections in the (Q_{xy}, Q_z) plane. Because of the 2D polycrystalline nature of the monolayer, the azimuthal angle between the peaks cannot be determined. (D) Projection of hydrocarbon tails onto a plane normal to the chain direction, showing the rhombus unit cell (shaded) with an angle γ, and the equivalent centered rectangular cell (dotted line).[21]

indicates a short-range order with an average d spacing $= 4.8$ Å. The out-of-plane GIXD peaks at different Q_z, and their dependence on pressure, show that the molecules in the monolayer form a 2D liquidlike state.

The diffraction pattern of C20-SP in the (Q_{xy}, Q_z) plane consists of two prominent peaks, one at $k_{z,f} = 0$ (where $k_{z,f} = k_0 \sin \beta$) and one centered at $k_{z,f} = 0.5$ Å^{-1} as shown in Figure 5A. The two peaks are due to the distortion of the hexagonal symmetry to the rhombus. The rhombus is defined by two parameters, an angle, γ, and a lattice constant, a, which determine $Q_{(1,-1)} = (2\pi)/(a \sin \gamma)$ and $Q_{(0,2)} = (2\pi)/(a \sin \gamma)(2(1 + \cos \gamma))^{1/2}$, using the equivalent centered rectangular lattice indexing. Because of the polycrystalline nature of the monolayer, the diffraction provides only the modulus of the two Bragg reflections, and therefore two sets of lattice parameters that equally fit the data are valid, as given in Table 2. The 2D orthorhombic ordering of the chains is depicted by the projection of CH$_2$ groups in a plane normal to the hydrocarbon chain axis in Figure 5. Rod-scan analysis of the two peaks using eq 2 and $F(Q_z) = \sin(Q_z l/2)/(Q_z l/2)$, where l is the length of the diffracting entities (the hydrocarbon chains in the present study), shows this plane is tilted with respect to the liquid surface. The best fits to the rod scan with a uniform chain tilt using model 1 or model 2 (i.e., tilt direction toward nearest neighbors or next nearest neighbors, respectively) described above are of the same quality. The parameter l in these fits is approximately 10 Å,

Table 2. Position of Observed Bragg Reflections Due to the In-Plane Ordering of Hydrocarbon Chains in C20-SP Monolayers[a]

	observed peaks		model 1			model 2		
π (mN/m)	Q_1 (Å^{-1})	Q_2 (Å^{-1})	a (Å)	b (Å)	A (Å^2)	a (Å)	b (Å)	A (Å^2)
0.2	1.4489	1.4010	5.240	8.673	22.722	4.954	8.970	22.218
1.0	1.4627	1.4161	5.181	8.591	22.257	4.909	8.874	21.781
10	1.4642	1.4246	5.141	8.582	22.062	4.912	8.821	21.662
20	1.4766	1.4483	5.043	8.510	21.458	4.883	8.677	21.182
32	1.4921	1.4460	5.072	8.422	21.360	4.814	8.690	20.917

[a] The two observed peaks labeled Q_1 and Q_2 have maximum intensity at the horizon $\beta = 0$ and off the horizon at a finite angle β, respectively. The observation of two peaks indicates a distorted hexagonal symmetry that is equivalent to a centered orthorhombic symmetry with lattice parameters a and b and a molecular area A. Because of the polycrystalline nature of the monolayer, the two peaks are insufficient in determining unique lattice parameters, but provide the parameters of two possible models. Q_1 and Q_2 correspond to the $(0,2)$ and $(1,-1)$ for model 1, and vice versa for model 2.
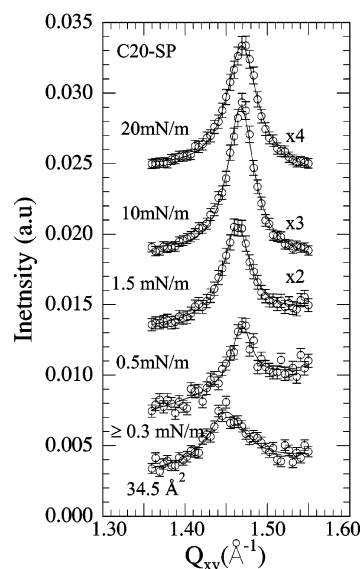
Figure 6. Diffraction patterns at $k_{z,f} = 0$ for C20-SP showing the variation of the Bragg peak with surface pressure. Because of the spontaneous condensation into nearly crystalline microdomains, a Bragg reflection is observed upon spreading the monolayer at vanishingly low surface pressures (very low densities). This is a common effect to other derivatives of sphingosine[6,7] due to strong hydrogen bonds at the headgroup region.[21]

consistent with a chain-slab split into two, one densely packed and crystalline and the other randomly digitated and disordered. The slab associated with the chains next to the gas interface is less dense, as it is digitated and therefore cannot be crystalline. The tilt angle of the chains with respect to the surface normal is $17-20°$, with no distinction between the two tilt directions.

Figure 6 shows the variation of the in-plane diffraction pattern for various surface pressures. An important result in this respect is the observation of a Bragg reflection at very small surface pressures (below 0.3 mN/m) at an isothermal molecular area of ~34.5 Å^2, as compared to that of $22.2-22.7$ Å^2 extracted from the GIXD (see Table 2). This is strong evidence for the spontaneous clustering of these molecules into crystalline microdomains at very low densities. Similar observations have been reported for C18-ceramide at the air/water interface.[6] Such sphingolipid microdomains in cellular membranes can be the precursors of lipid rafts to which proteins can be attached and moved around to specific sites during signal transduction.[4] Sphingolipids, with their strong hydrogen bonds among nearest

neighbors and with water molecules, tend to phase-separate from unsaturated lipids,[9] rendering them lateral mobility and solubility that can get them inside the cell as well. Diffraction patterns from C18-SP at very low surface pressures also show a weak peak, indicating that this clustering is not unique to C20-SP and therefore is a result of the strong bonding (hydrogen) in the headgroup region. While it is tempting to associate the clustering of sphingolipids (C18-SP, C20-SP, and C18-ceramide, and C18-sphingomyelin) to lipid rafts, it should be pointed out that it was suggested that the constituents of these rafts are glycosphingolipids and cholesterol,[4] which are much more complicated than the simple sphingosines presented here. What is argued here is that the clustering originates in sphingosine due to strong hydrogen bonds in the headgroup region and these bonds can be in action also in the more complex sphingolipid derivatives.

Conclusions

The present synchrotron X-ray studies and surface pressure versus molecular area isotherms of C18-SP and C20-SP spread at air/water interfaces reveal interfacial properties that shed light on their functions in cellular membranes. In particular, we find that C18-SP is marginal in its ability to form a homogeneous monolayer, most likely due to its higher solubility in water, and that the slab at the water/molecule interface is broader than the sphingosine headgroup region, leading to digitated tails at the gas interface. Such corrugation, which was also observed in monolayers of sphingosine derivatives (i.e., C18-ceramide and C18-sphingomyelin;[6,9] skin tissue and myelin sheath constituents, respectively), enlarges the effective surface area of the monolayer and can strengthen leaflet−leaflet binding in a bilayer membrane configuration. Whereas C20-sphingosine forms a crystalline monolayer with structural characteristics that are dominated by hydrogen bonding in the headgroup (common to its sphingolipid derivatives), its natural counterpart C18-sphingosine forms a disordered liquidlike metastable monolayer. To maintain a metastable monolayer during the X-ray scattering studies, C18-SP has to be spread in excess with a floating reservoir on the water surface, due to the high dissolution rate into the water subphase. Such marginal affinity to forming a monolayer is an important property which can allow sphingosine clusters to easily migrate to and from the membrane and the bulk solution, to perform their tasks as secondary messengers. We hypothesize that the attractive forces between the amino-alcohol headgroup and water molecules are comparable to the opposing hydrophobic forces between hydrocarbon chains and water, leading to the marginal solubility of C18-SP in water, and that the addition of two CH_2 hydrophobic groups, as in C20-SP, increases the hydrophobic forces, thereby lowering the solubility of C20-SP as compared to that of C18-SP.

The X-ray scattering studies also show that both C20- and C18-sphingosines have a tendency to cluster and form microcrystals or microdomains at very low densities due to strong hydrogen bonds at the headgroup region. A weak but measurable effect of the monolayer on the structure factor of water was also observed, suggesting a significant interaction between the headgroup and water molecules. Such lipid microdomains can serve as substrates for proteins that can bind either through their hydrophobic regions to the corrugated hydrocarbon chain surface by interdigitation or through their hydrophilic protein regions to the headgroups directly by hydrogen bonds or indirectly by interacting with intermediating bound water molecules.

JA028292M